Three-energy focusing Laue monochromator for the diamond light source x-ray pair distribution function beamline I15-1

John P. Sutter, Philip A. Chater, Michael R. Hillman, Dean S. Keeble, Matt G. Tucker, and Heribert Wilhelm

Citation: AIP Conference Proceedings **1741**, 040005 (2016); doi: 10.1063/1.4952877
View online: http://dx.doi.org/10.1063/1.4952877
View Table of Contents: http://scitation.aip.org/content/aip/proceeding/aipcp/1741?ver=pdfcov
Published by the AIP Publishing

Three-Energy Focusing Laue Monochromator for the Diamond Light Source X-Ray Pair Distribution Function Beamline I15-1

John P. Sutter[1, a)], Philip A. Chater[1], Michael R. Hillman[1], Dean S. Keeble[1], Matt G. Tucker[1,2], and Heribert Wilhelm[1]

[1]*Diamond Light Source Ltd, Harwell Science and Innovation Campus, Chilton, Didcot, Oxfordshire OX11 0DE, United Kingdom*
[2]*ISIS Neutron and Muon Source, Science and Technology Facilities Council, Rutherford Appleton Laboratory, Harwell Oxford, Didcot, Oxfordshire OX11 0QX, United Kingdom*

[a)]Corresponding author: john.sutter@diamond.ac.uk

Abstract. The I15-1 beamline, the new side station to I15 at the Diamond Light Source, will be dedicated to the collection of atomic pair distribution function data. A Laue monochromator will be used consisting of three silicon crystals diffracting X-rays at a common Bragg angle of 2.83°. The crystals use the (1 1 1), (2 2 0), and (3 1 1) planes to select 40, 65, and 76 keV X-rays, respectively, and will be bent meridionally to horizontally focus the selected X-rays onto the sample. All crystals will be cut to the same optimized asymmetry angle in order to eliminate image broadening from the crystal thickness. Finite element calculations show that the thermal distortion of the crystals will affect the image size and bandpass.

INTRODUCTION

Diamond Light Source is an X-ray synchrotron facility of electron energy 3 GeV with beamlines dedicated to studies of materials using imaging, spectroscopy and diffraction. Diffraction is particularly widely applied because it provides information on atomic positions in complex materials. Diamond's repertoire of techniques will soon be further expanded by the I15-1 side station on the Extreme Conditions beamline I15. I15-1 will take beam from the multi-pole superconducting wiggler for I15, 1.5 mrad off the central axis (see Fig. 1(a)). The high energies available in its wide energy profile (20-80 keV) make it a suitable source for a versatile X-ray pair distribution function (X-PDF) beamline. From the measured X-PDF data, local atomic structure correlations can be calculated. Unlike typical powder diffraction, which allows only examination of materials that have long-range order, X-PDFs can be obtained from both ordered and disordered materials, including glasses and liquids, because they measure local, medium and average long-range atomic structures simultaneously. There are many industrially and commercially important processes that are influenced by local atomic environments, such as catalytic processes, nuclear waste storage, digital storage media, multiferroic transitions, heavy metal sequestration in clays, and the absorption of medications in the human body.

A high photon energy is required for X-PDF measurements as the resolution of the data obtained depends primarily on the maximum measured length of the scattering vector, $|\mathbf{Q}|_{\max} \propto E \sin\theta_{\max}$. In addition, an X-ray beam with an adequate bandwidth must be selected from the broad-band wiggler source. A 2% bandwidth is sufficient to measure interatomic distances up to about 10 Å, whereas a 0.2% bandwidth gives access up to 100 Å (Fig. 1(b)), though inevitably this larger range is achieved at a cost to the available photon flux. A tunable bandpass will therefore allow users to optimize their individual experiments. Finally, the horizontally and vertically divergent X-ray beam must be focused so that 2D scattering data can be collected with sufficient resolution. I15-1 will use a spot

Proceedings of the 12th International Conference on Synchrotron Radiation Instrumentation – SRI2015
AIP Conf. Proc. 1741, 040005-1–040005-4; doi: 10.1063/1.4952877
Published by AIP Publishing. 978-0-7354-1398-6/$30.00

size of approximately 700 μm (horizontal) × 20 μm (vertical) through the combination of a horizontally focusing bent Laue monochromator (BLM) and a vertically focusing multilayer mirror. This beam size is adequate for X-PDF measurements and is the best that can be obtained within the geometrical constraints of I15-1. Symmetrical beam sizes may be delivered by a combination of horizontal collimation and vertical de-focusing.

CRYSTAL DESIGN

The Bragg reflections were determined by the beamline geometry and the required operating photon energies. The BLM will contain three float-zone silicon single crystals mounted in a crystal cage for angular and meridional bending adjustment (Fig. 1(c)). Each crystal will be oriented to a different Bragg reflection: (1 1 1), (2 2 0) and (3 1 1). The reflections will be in the Laue (transmission) geometry, for which the beam footprint and hence the required crystal size are much less than in Bragg (reflection) geometry. They will all deflect the monochromated beam horizontally through an angle of $2\theta_B = 5.66°$ and thus will select the photon energies 40, 65 and 76 keV respectively. The crystals have been manufactured by Crystal Scientific (UK) Ltd (Alnwick, United Kingdom) and have been installed in a crystal cage assembly manufactured by FMB Oxford Ltd (Oxford, United Kingdom). The remaining parameters to be optimized were the asymmetry angle of the reflections and the crystal bending radius, which are determined by the two types of focusing in meridionally bent Laue crystals [1, 2].

First, if one assumes a divergent polychromatic beam emitted by a point source a distance p from the crystal, the rays diffracted by the bent Laue crystal will meet at a focus at a distance q from the crystal given by

$$q = -p\left(\frac{R\cos(\theta_B+\varphi)}{2p - R\cos(\theta_B-\phi)}\right), \tag{1}$$

where θ_B is the Bragg angle, φ is the asymmetry angle and R is the bending radius. Here the sign conventions are: $R > 0$ if the concave side of the bent crystal faces the source, $\varphi > 0$ if the diffraction vector is rotated toward the source, $q > 0$ if the focus is real. Secondly, a bent Laue crystal will separate the energies of a perfectly collimated polychromatic beam of zero spatial extent ("pencil beam") into a fan and then refocus them at a distance Q:

$$Q = R\left(\frac{\sin 2\theta_B}{-2\sin(\theta_B-\varphi)+(1+\nu)\sin 2\varphi\cos(\theta_B-\varphi)}\right), \tag{2}$$

where the crystal has been assumed to have an isotropic Poisson ratio $\nu = 0.2$. Eq. (2) is like Eq. (4) in [1] but accounts for the inequality of the rotation of the diffracting planes and that of the surface normal along the ray paths for general φ. If $q \neq Q$, there will be a thickness-dependent broadening of the intended image at q. However, if φ is adjusted to set $q = Q$, then this broadening is eliminated, and the crystal thickness T can be set to a convenient value (here $T = 3.0$ mm) for optimal mounting and cooling without degrading the focal quality. For each crystal we have chosen p = 26.64 m, q = 8.96-9.96 m and $\varphi = -2.61°$. R will be adjustable from −35 m to −25 m. Because the wiggler radiates along its whole length, the effective photon source size can be estimated as the wiggler length times the viewing angle, i.e. (24 periods)(60 mm/period)(1.5 mrad) = 2.16 mm, considerably larger than the 300 μm horizontal electron beam width. The geometrical demagnification q/p then reduces this to a focal spot size of 730 μm. More precise ray-tracing calculations with SHADOW [3], which account for the real properties of the electron beam and the wiggler, yield a horizontal focal spot size of 696 μm.

The bandpass of the diffracted rays for both types of focusing must also be considered. For the divergent polychromatic beam, rays diffracted from the same depth within the crystal cover a bandwidth that is proportional to the horizontal divergence $\Delta\theta_H$:

$$\frac{\Delta E_{div}}{E} = \Delta\theta_H\left|1 - \frac{p}{R\cos(\theta_B-\varphi)}\right|\cot\theta_B\ , \tag{3}$$

while rays diffracted from the polychromatic "pencil beam" cover a bandwidth proportional to the thickness T [1]:

$$\frac{\Delta E_T}{E} = \frac{T}{|R|}\cot\theta_B\left|-\tan(\theta_B-\phi)+\frac{1}{2}(1+\nu)\sin 2\phi+\frac{1}{2}\tan\theta_B\left[(1-\nu)+(1+\nu)\cos 2\phi\right]\right|. \tag{4}$$

Here, the second contribution, being only 2.44×10^{-4} at $R = -25$ m, is negligible. The first yields a bandpass ~ 2% for $\Delta\theta_H = 0.5$ mrad, the maximum horizontal width of the white beam slits, with narrower slits yielding smaller bandwidths. Ray traces using SHADOW [3] give a bandwidth of 750 eV for 40 keV X-rays (1.88%).

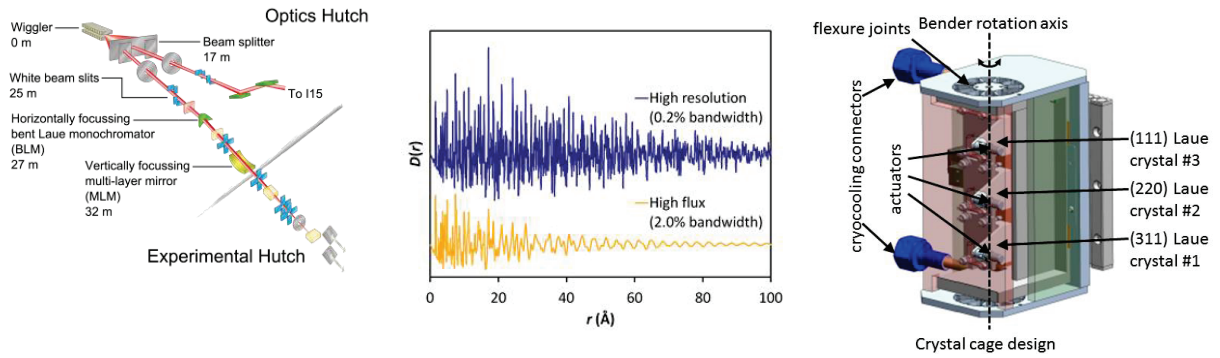

(a) (b) (c)

FIGURE 1. (a) Schematic of the I15-1 side station. The divergent X-ray beam (0.5 × 0.13 mrad^2) will be horizontally and vertically focused by the bent Laue monochromator and the multi-layer mirror, respectively. (b) Simulated X-PDF of $AlPO_4$ at two bandwidths. A smaller bandwidth gives access to larger interatomic distances. (c) Crystal cage design (FMB Oxford Ltd). The bender rotation axis allows the crystals to be pushed against actuators and hence to achieve the bending.

THERMAL FINITE ELEMENT ANALYSIS

The deformation of the crystals under the thermal load induced by the incident wiggler beam has been modeled by finite element analysis (FEA) using the software package ANSYS [4]. Although the typical electron beam current in the Diamond storage ring is 300 mA, for these simulations 550 mA was assumed in order to leave room for future upgrades. The base of each crystal, which will be in contact with the cryogenically cooled heat exchanger, was assumed here to be at a fixed temperature of 80 K. The thermal load will vary as a function of depth into the crystal; for simplicity each crystal was divided into three layers and a different thermal load applied to each layer. The front layer (facing the incident beam) was 0.5 mm thick, the middle layer 1.0 mm thick and the back layer 1.5 mm thick. The two cases considered here are described in Table 1. Beam currents of 40% (Case #1) and 60% (Case #2) of the maximum expected value of 550 mA have been modelled.

TABLE 1. The two beam current cases considered for finite element calculations. Beam width and size are given as horizontal × vertical. The three tabulated heat load densities (HLD) are proportional to their values at the full current of 550 mA.

Case	Beam size (mrad)	Illuminated area (mm)	% of full current	Front HLD (W/mm^3)	Middle HLD (W/mm^3)	Back HLD (W/mm^3)	Total power (W)
#1	0.40 × 0.13	10.6 × 3.5	40	2.22	1.48	0.93	146
#2	0.20 × 0.13	5.3 × 3.5	60	3.34	2.23	1.40	110

A summary of the results of the FEA analysis is given in Table 2 and the temperature distributions are shown in Fig. 2(a-c). The calculated displacements of the nodes of the elements in the FEA model were converted into alterations in the spacing and meridional tilt of the diffracting atomic planes as explained in [5]. Though somewhat noisy because the cell size is finite, the data show that under thermal load the diffracting atomic planes take an hourglass shape with its waist at a depth of approximately 2.25 mm (Fig. 2(d)). Distortions at the front and back surfaces of the crystal in Case #2 are shown in Fig. 3; a worst-case estimate of the effects on the performance can be calculated from their peak-to-valley ranges δq in Table 2. δq is larger in Case #2 because the beam size on the crystal is half its value in Case #1 while the total power is only 25% less, thus increasing the thermal gradients. The resulting focal broadening s, which for a point source could be estimated geometrically as $s = B_H(\delta q / q)\cos 2\theta_B$ where B_H is the horizontal incident beam size on the crystal, is substantial. The deformation's contribution to the bandpass is less severe but still noticeable compared to the theoretical bandpasses without thermal deformation. The incident beam will thus require significant filtering to further reduce the heat load on the crystals.

TABLE 2. Summary of results of FEA calculations for the two cases in Table 1. T_{max} is the maximum temperature within the crystal volume. δq is the peak-to-valley variation in the focusing distance with depth caused by the thermal distortion. s is the geometrically estimated focal broadening at a focal distance q = 9 m. B is the quadrature sum of s with the 0.7 mm horizontal focal spot size for an undistorted crystal. $\delta\lambda_{def}/\lambda$ is the estimated increase in bandpass caused by the thermal distortion. $\delta\lambda_{theor}/\lambda$ is the theoretical bandpass of the undistorted crystal.

Case	T_{max} (K)	δq (m)	s (mm)	B (mm)	$\delta\lambda_{def}/\lambda$ (%)	$\delta\lambda_{theor}/\lambda$ (%)

#1	170	±0.74 m	0.871	1.115	0.15	1.6
#2	141	±1 m	0.588	0.911	0.10	0.8

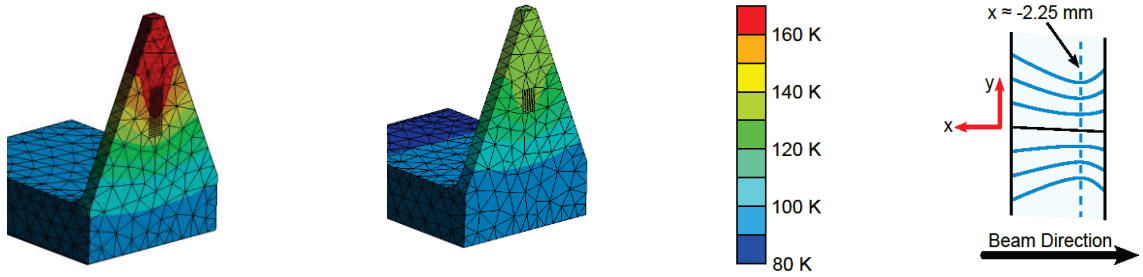

(a) (b) (c) (d)

FIGURE 2. ANSYS thermal finite element calculations: (a) Temperature distribution in Case #1. (b) Temperature distribution in Case #2. The mesh is indicated by the black lines. Note that on the beamline the tip of each crystal would point horizontally. (c) Color scale of temperatures in (a) and (b). (d) Schematic of the hourglass shape of the thermally distorted diffracting planes (blue curves). *X* indicates depth and *Y* points along the meridional direction. The diffracting planes are parallel at $x \approx -2.25$ mm.

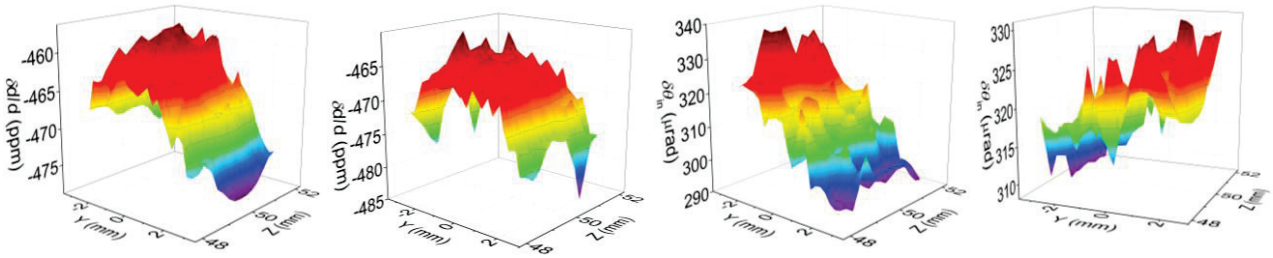

(a) (b) (c) (d)

FIGURE 3. For Case #2: (a) Relative change in spacing of diffracting atomic planes from room temperature value in parts per million at front surface. (b) Same as (a) for back surface. (c) Change in tilt of diffracting atomic planes from room temperature value in μrad at front surface. (d) Same as (c) for back surface.

Commissioning the bent Laue monochromator with X-rays will provide a quantitative measure to verify the design and modelling efforts. Once full user operation begins, the synchrotron community will gain a valuable new instrument for the analysis of many types of materials.

ACKNOWLEDGMENTS

The authors thank Dave Barber, Nanna Heiberg, Abi Marchant, and Steve Syme of FMB Oxford Ltd for the design of the BLM and Simon Cockerton of Crystal Scientific (UK) Ltd for manufacturing the crystals.

REFERENCES

1. P. Suortti, W. Thomlinson, D. Chapman, N. Gmür, D. P. Siddons and C. Schulze, Nucl. Instrum. Methods Phys. Res. A **336**, 304-309 (1993).
2. C. Schulze, U. Lienert, M. Hanfland, M. Lorenzen and F. Zontone, J. Synchrotron Rad. **5**, 77-81 (1998).
3. M. Sánchez del Río, N. Canestrari, F. Jiang and F. Cerrina, J. Synchrotron Rad. **18**, 708-716 (2011).
4. ANSYS Inc. (2014), ANSYS® Workbench™, Release 15.
5. J. P. Sutter, T. Connolley, T. P. Hill, H. Huang, D. W. Sharp and M. Drakopoulos, J. Synchrotron Rad. **15**, 584-592 (2008).